

# First-Principles Calculation of the Real-Space Order Parameter and Condensation Energy Density in Phonon-Mediated Superconductors

A. Linscheid,<sup>1</sup> A. Sanna,<sup>1</sup> A. Floris,<sup>2</sup> and E. K. U. Gross<sup>1</sup>

<sup>1</sup>Max-Planck-Institut für Mikrostrukturphysik, Weinberg 2, D-06120 Halle, Germany

<sup>2</sup>CIC Energigune, Albert Einstein 48, 01510 Miñano (Álava), Spain

(Received 11 September 2014; revised manuscript received 12 July 2015; published 28 August 2015)

We show that the superconducting order parameter and condensation energy density of phonon-mediated superconductors can be calculated in real space from first principles density functional theory for superconductors. This method highlights the connection between the chemical bonding structure and the superconducting condensation and reveals new and interesting properties of superconducting materials. Understanding this connection is essential to describe nanostructured superconducting systems where the usual reciprocal space analysis hides the basic physical mechanism. In a first application we present results for MgB<sub>2</sub>, CaC<sub>6</sub> and hole-doped graphane.

DOI: 10.1103/PhysRevLett.115.097002

PACS numbers: 74.20.Pq, 74.70.Ad, 74.70.Wz, 74.78.Na

In the last decades, many theoretical and experimental studies about superconductors, especially those with a large critical temperature ( $T_c$ ), have highlighted, as crucial for the superconducting (SC) condensation, very special features in reciprocal space, like specific phonons and/or electronic bands. Cuprates, pnictides, MgB<sub>2</sub>, and intercalated graphite are all relevant examples. Since the SC condensation occurs for electron pairs of opposite momenta [1–3], it seems natural to describe it in reciprocal space [3], e.g., by characterizing the momentum dependence of the SC gap. This has been the traditional way of analyzing superconductivity.

There are, however, important features, such as the chemical bonding structure, which are not easily understood in  $\mathbf{k}$  space. Since the electrons, within the bonds, are found to have a different degree of localization and considering that this bonding structure also determines the electron-phonon coupling, a real-space analysis can reveal essential information for superconductivity. In fact, in the class of MgB<sub>2</sub>-type superconductors the strength of the  $\sigma$  bond was found to correlate with the magnitude of the critical temperature [4,5].

The preferable space for analyzing superconductors should, in fact, depend on the material. In a conventional superconductor like bulk lead, remarkable anisotropies in reciprocal space have been observed and predicted [6–9]. However, many bulk materials and, even more so, systems with a broken periodicity in one or two dimensions—surfaces, 2D-systems, interfaces, nanostructures—clearly exhibit strong anisotropies and selective features also in real space, where the SC transition might involve only specific atoms, layers, and chemical bonds. This suggests that characterizing how the SC order parameter behaves in real space and identifying the specific chemical structures that enhance or weaken the SC condensation can be important to set new connections between superconductivity and simple chemistry, laying the ground for rational

design. Clearly, in nanostructured systems, a real-space analysis seems much more intuitive and revealing, due to the folding of the Brillouin zone.

In this Letter we develop a scheme to calculate the SC order parameter in real space. A detailed analysis of this quantity and the corresponding SC pairing potential is performed for three strongly anisotropic systems, as MgB<sub>2</sub>, CaC<sub>6</sub>, and hole-doped graphane (C<sub>2</sub>H<sub>2</sub>). Further, the connection between the stability of the SC state and the local chemical environment is established by introducing a condensation energy density which is defined and computed for the three considered superconductors. Several phenomenological or model approaches, such as the Ginsburg-Landau theory [10,11], the Bogoliubov–de Gennes (BdG) equations [12], lattice models, and others [13] were used as models to achieve real-space descriptions of mesoscopic systems in complex geometries [14–16] and topologies [17]. The present work aims to take a step further and obtain a description of real-space quantities in a completely *ab initio* fashion, thereby also filling the gap between large scale models and microscopic approaches typically framed in the reciprocal space.

We develop our real-space description in the framework of the fully *ab initio* density functional theory for superconductors (SCDFT) [9,18–25]. The real-space description can in principle be obtained also starting from alternative approaches such as the Eliashberg theory [26]. However, some distinctive features of SCDFT, as compared to many-body perturbation theory are (i) the absence of semi-empirical parameters like the Coulomb pseudopotential  $\mu^*$ , commonly used in Eliashberg implementations to reduce the computational cost, and (ii) the possibility of performing analytically and exactly the frequency integrations implied by the electron-phonon (*e*-ph) interaction retardation effects, a fact that makes this theory computationally much cheaper than other many-body approaches.

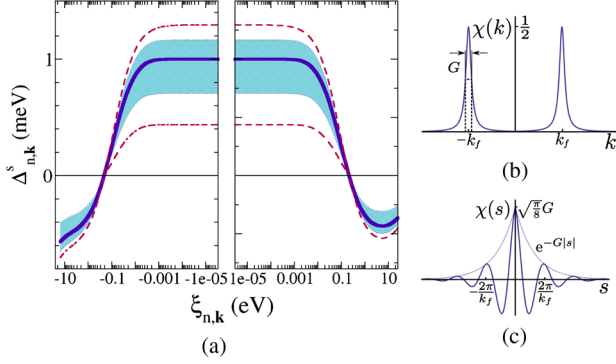


FIG. 1 (color online). (a) Superconducting gap  $\Delta_s^{nk}$  versus energy  $\xi_{nk}$  on a logarithmic scale of an isotropic (dark blue line) and an ideal two gap (dashed red) system. In real materials,  $\mathbf{k}$  anisotropy leads to a continuous set of  $\Delta_s^{nk}$  at a given energy (shaded area). (b) Typical Lorentz peak of  $\chi(k)$  in a 1D model system around the Fermi vectors  $\pm k_F$  with width  $G$ . Its real-space transform [panel (c)] shows oscillations of periodicity  $2\pi/k_F$  and exponential damping  $e^{-G|s|}$ .

This allows us to calculate the SC properties in much larger or complex systems.

In SCDFT, both the electronic density  $n(\mathbf{r})$  as well as the *exact* SC order parameter  $\chi(\mathbf{r}, \mathbf{r}')$  of the interacting system are reproduced by a SC noninteracting Kohn-Sham (KS) system where the exchange-correlation (xc) effects on superconductivity are included via the pairing potential  $\Delta_s(\mathbf{r}, \mathbf{r}')$ , functional of  $n(\mathbf{r})$ , and  $\chi(\mathbf{r}, \mathbf{r}')$ .  $\Delta_s(\mathbf{r}, \mathbf{r}')$  does not have, in principle, a direct physical meaning. However, in the approximation for the xc energy functional introduced in Ref. [19], its diagonal matrix elements with respect to the normal state (NS) KS Bloch orbitals  $\Delta_s^{nk} = \langle \varphi_{n\mathbf{k}} | \Delta_s | \varphi_{n\mathbf{k}} \rangle$  modify the electronic spectrum according to a BCS expression of the quasiparticle energies  $E_{n\mathbf{k}} = \sqrt{\xi_{n\mathbf{k}}^2 + |\Delta_s^{nk}|^2}$ , where  $\xi_{n\mathbf{k}}$  are eigenvalues of the NS-KS system and  $n$  and  $\mathbf{k}$  are band and Bloch vector indexes, respectively. This is the reason why  $\Delta_s$  has been very successfully interpreted [21,23,27] as a mean field SC gap function, in the same sense as the NS-KS eigenvalues are interpreted as approximate quasiparticle energies. The gap function is obtained by solving the self-consistent equation

$$\Delta_s^{nk} = \mathcal{Z}_{n\mathbf{k}} \Delta_s^{nk} - \sum_{n'\mathbf{k}'} \mathcal{K}_{n'\mathbf{k}'}^{n\mathbf{k}} \frac{\tanh(\frac{\beta}{2} E_{n'\mathbf{k}'})}{2E_{n'\mathbf{k}'}} \Delta_s^{n'\mathbf{k}'}, \quad (1)$$

where the effects of the Coulomb and the retarded  $e$ -ph interactions [28] are included in the kernels  $\mathcal{Z}$  and  $\mathcal{K}$ , functionals of the densities.  $\beta$  is the inverse temperature. The matrix elements of the order parameter (OP) in KS states are then expressed in terms of  $\Delta_s$  as

$$\chi_{n\mathbf{k}} \equiv \frac{\Delta_s^{nk}}{2|E_{n\mathbf{k}}|} \tanh\left(\frac{\beta}{2} E_{n\mathbf{k}}\right). \quad (2)$$

The typical energy dependence of  $\Delta_s^{nk}$  and  $\chi_{n\mathbf{k}}$  is sketched in Fig. 1(a). If the system shows time-reversal symmetry, these functions can be chosen to be real and positive at the Fermi energy ( $E_F$ ), where both functions show a sharp peak. However, due to the Coulomb repulsion, beyond the phononic energy scale the gap function changes sign and exhibits a long and rather deep negative tail extending at high energies. In the Supplemental Material [30], we review in detail how the Coulomb renormalization mechanism [38,39] operates in the SC-KS system. A negative tail is expected also in  $\chi_{n\mathbf{k}}$  [Eq. (2)], but it is strongly suppressed by the  $(2|E_{n\mathbf{k}}|)^{-1}$  factor.

The order parameter and the gap function can be expressed in real space using the NS KS Bloch basis

$$\chi(\mathbf{R}, \mathbf{s}) = \sum_{n\mathbf{k}} \chi_{n\mathbf{k}} \varphi_{n\mathbf{k}}\left(\mathbf{R} + \frac{\mathbf{s}}{2}\right) \varphi_{n\mathbf{k}}^*\left(\mathbf{R} - \frac{\mathbf{s}}{2}\right), \quad (3)$$

$$\Delta_s(\mathbf{R}, \mathbf{s}) = \sum_{n\mathbf{k}} \Delta_s^{nk} \varphi_{n\mathbf{k}}\left(\mathbf{R} + \frac{\mathbf{s}}{2}\right) \varphi_{n\mathbf{k}}^*\left(\mathbf{R} - \frac{\mathbf{s}}{2}\right), \quad (4)$$

where we introduced the center of mass coordinates  $\mathbf{R} \equiv (\mathbf{r} + \mathbf{r}')/2$ ,  $\mathbf{s} \equiv \mathbf{r} - \mathbf{r}'$ , which is very convenient for the analysis presented below. By applying the Bloch theorem, it is easily seen that both  $\chi(\mathbf{R}, \mathbf{s})$  and  $\Delta_s(\mathbf{R}, \mathbf{s})$  are lattice periodic in  $\mathbf{R}$ , while they show Friedel-like oscillations as a function of  $\mathbf{s}$ . The presence of these oscillations can be understood by considering a 1D homogeneous model system, with plane waves as Bloch functions. In this case,  $\chi(\mathbf{s})$  reduces to the Fourier transform of  $\chi_{n\mathbf{k}}$ . Modeling  $\chi_{n\mathbf{k}}$  as a Lorentzian function peaked at the Fermi vectors  $k_f$  and  $-k_f$  [Fig. 1(b)], we see that its transform [Fig. 1(c)] shows oscillations whose period and damping are related to the Fermi momentum modulus and  $\chi_{n\mathbf{k}}$  width, respectively. The real-space computation of  $\chi$  is realized in two steps, first by solving Eq. (1) and extracting the matrix elements in Eq. (2), and second by performing the  $n, \mathbf{k}$  integration in Eq. (4).

A brief summary of the studied materials is presented below (see also the Supplemental Material [30]). MgB<sub>2</sub> has two Fermi surface (FS) sheets, associated with  $\sigma$  and  $\pi$  electrons and coupled very differently to the phonons. This anisotropic material is a well-known prototype of a two-gap system: the cylindrical FS arising from the  $B$ - $B$ - $\sigma$  bonds shows a SC gap three times larger than the  $\pi$ -related one [40]. A former SCDFT study [21] reported a critical temperature and a gap structure in good agreement with the experimental observations [41].

The second system considered is a hole-doped graphane single layer, recently studied within SCDFT [42]. Here, the cylindrical FS arises mainly from the C  $\sigma$  bonds, strongly coupled to the phonon modes [43]. Finally, we will investigate CaC<sub>6</sub>, a material where a  $T_c = 9.4$  K was obtained in SCDFT, slightly below the experimental 11.5 K [23,44]. Compared to MgB<sub>2</sub> and graphane, CaC<sub>6</sub> has a complex FS with a strong atomic orbital character.

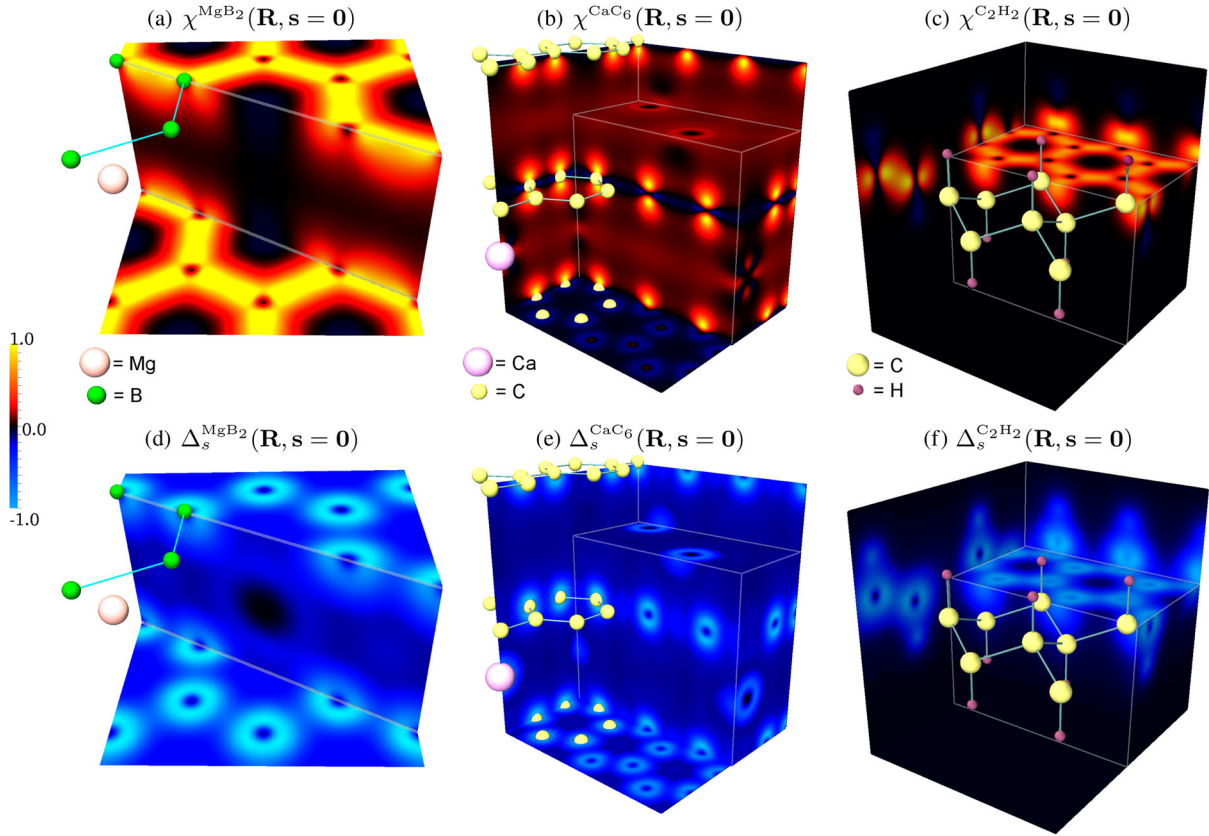


FIG. 2 (color online). Normalized  $\chi(\mathbf{R}, \mathbf{0})$  for MgB<sub>2</sub> (a), CaC<sub>6</sub> (b), and C<sub>2</sub>H<sub>2</sub> (c) (See also Refs. [30,45]). States relevant for superconductivity appear in the plots. We show the normalized  $\Delta_s(\mathbf{R}, \mathbf{0})$  in MgB<sub>2</sub> (d) CaC<sub>6</sub> (e) and C<sub>2</sub>H<sub>2</sub> (f). For small separations  $|\mathbf{s}|$  the pair potential is dominated by the screened Coulomb interaction.

The outer parts are dominated by C- $p_z$  orbitals, while the central spherical one mostly by Ca- $d_{z^2}$  and Ca- $s$  orbitals. The strongly anisotropic  $e$ -ph coupling is due to Ca vibrations, while C modes give a smaller, homogeneous contribution. As a result, CaC<sub>6</sub> does not show distinct multiband superconductivity but a rather anisotropic gap in  $\mathbf{k}$  space [27].

In Fig. 2 we show the plots of  $\chi(\mathbf{R}, \mathbf{s} = 0)$  and  $\Delta_s(\mathbf{R}, \mathbf{s} = 0)$  for the three considered systems, at  $T = 0.01$  K. We consider only a low temperature limit since  $T$  acts as a spatially homogeneous scale factor. Although related to each other, the two functions highlight different properties. Since  $\chi_{n\mathbf{k}}$  is strongly peaked around the FS and only slightly negative elsewhere,  $\chi(\mathbf{R}, \mathbf{0})$  reveals the structure of the electronic states close in energy to  $E_F$ , weighted by the relative strength of the  $e$ -ph coupling [Eq. (4)].  $\Delta_s^{n\mathbf{k}}$ , instead, is much broader in energy and its long negative tail overbalances the positive phonon contribution, dominating the  $\Delta_s(\mathbf{R}, \mathbf{0})$  overall behaviour and giving more weight to the high energy KS states. Via the mechanism described following Eq. (2), these are involved in the Coulomb renormalization. Therefore,  $\chi(\mathbf{R}, \mathbf{0})$  is positive almost everywhere (red to yellow), negative only in regions where the Coulomb renormalization dominates while  $\Delta_s(\mathbf{R}, \mathbf{0})$  is negative (light to dark blue).

Specifically, in MgB<sub>2</sub> [Fig. 2(a)] we observe from  $\chi(\mathbf{R}, \mathbf{0})$  how the  $e$ -ph pairing is dominated by the B  $\sigma$  states, and much less by the  $\pi$  states, that are barely visible. A change of sign in the center of the Boron hexagon, yet with a very small magnitude, indicates that this region plays a role in the Coulomb renormalization. Regions in the unit cell (U.c.) contributing to this mechanism are, however, highlighted better by  $\Delta_s(\mathbf{R}, \mathbf{0})$  [Fig. 2(d)]. Clearly distinguishable are the ring-shaped regions around the B atoms, overimposed on a homogeneous background, respectively originating from states below and above  $E_F$ . The region of the Mg atom gives a negligible contribution (black region).

The  $\chi(\mathbf{R}, \mathbf{0})$  plot for CaC<sub>6</sub> [Fig. 2(b)] highlights instead a complex orbital character in the  $E_F$  region that mirrors the complexity of the  $e$ -ph coupling. Regions associated with C- $\pi$  states appear with the largest magnitude, while C- $\sigma$  regions provide Coulomb renormalization, and are again better seen in  $\Delta_s$  [Fig. 2(e)]. Ca- $d_{z^2}$  states are also clearly visible in the lower right corner of Fig. 2(b).

In graphane,  $\chi(\mathbf{R}, \mathbf{0})$  reflects the hexagonal bonding structure [Fig. 2(c)] similarly to MgB<sub>2</sub>; i.e., the C- $\sigma$  bond regions show the largest positive values. On the other hand, the regions of Coulomb renormalization shown by  $\Delta_s(\mathbf{R}, \mathbf{0})$  [Fig. 2(f)] are not only the carbon honeycomb lattice but have a strong contribution also the covalent

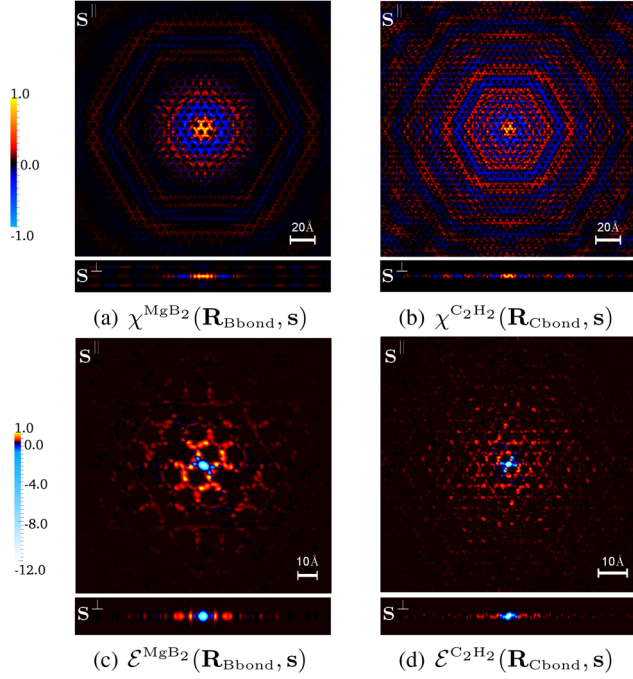


FIG. 3 (color online).  $s$  dependence of  $\chi(\mathbf{R}_0, \mathbf{s})$  [panels (a),(b)] and  $\mathcal{E}(\mathbf{R}_0, \mathbf{s})$  [(c) and (d)] in the  $xy$  plane and  $z$  direction.  $\mathbf{R}_0$  is located in a B– $\sigma$  bond in  $\text{MgB}_2$  and in a C– $\sigma$  bond in graphane. Maximal values are 49 and 77  $\mu/\text{U.c.}$  in (a) and (b) and 64 fRy/U.c.<sup>2</sup> and 120 fRy/U.c.<sup>2</sup> in (c) and (d), respectively. At  $s \approx 0$  a sharp negative peak in  $\mathcal{E}$  marks the onset of the Coulomb repulsion between paired electrons.

H–C– $p_z$  bonds, which do not participate in the phononic pairing. In a H–C– $p_z$  bond,  $\chi(\mathbf{R}, \mathbf{0})$  is out of phase (negative in Fig. 2(c) with respect to the C–C bond region, indicating that this bond renormalizes the Coulomb repulsion. This clearly illustrates how our *ab initio* real-space description is able to identify the chemical bonds that limit the suppressive nature of the long range Coulomb interaction on the SC condensation.

In the present nonlocal formulation we can investigate also the  $\mathbf{s}$  dependence of the Cooper pair wave function  $\chi(\mathbf{R}_0, \mathbf{s})$ .

In Fig. 3(a) we set  $\mathbf{R}$  in a  $\text{MgB}_2$  B–B bond and we plot  $\chi(\mathbf{R}_0, \mathbf{s})$  on the B plane. The shape we observe is given by the charge density at Fermi level, modulated by damped Friedel-like oscillations representing the 3D generalization of the 1D model of Figs. 1(b) and 1(c). Since the FS of both  $\text{MgB}_2$  and graphane is almost cylindrical, the oscillations lay in the boron plane. Here the envelope of  $\chi(\mathbf{R}_0, \mathbf{s})$  is given by a Bessel function of first kind [ $J_n(|k_r||s|)$  with  $k_r$  the radius of the FS cylinder and  $n=0$ ] times an exponential damping due to the small width of  $\chi_{n\mathbf{k}}$  around the Fermi level. In the out-of-plane direction ( $s_z$ ) destructive interferences lead to a rapid decay of  $\chi(\mathbf{R}_0, \mathbf{s})$ . For the same reason, in  $\text{CaC}_6$  (not shown) the more complicated FS results in a strong interference and no distinct oscillations are visible.

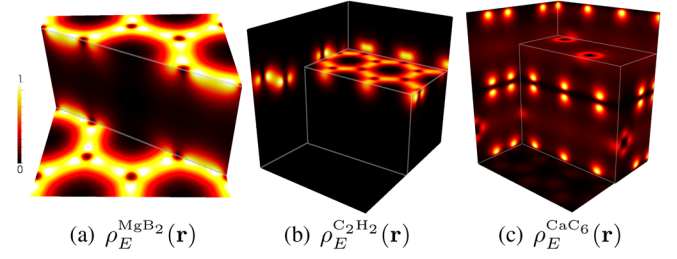


FIG. 4 (color online). Normalized, spatially resolved energy gain due to the condensation  $\rho_E(\mathbf{r})$  for  $\text{MgB}_2$  (a),  $\text{CaC}_6$  (b), and  $\text{C}_2\text{H}_2$  (c) (See also Ref. [47]). The structure is very similar to  $\chi(\mathbf{R}, \mathbf{0})$ , however, positive everywhere.

The gap function (not shown) features an oscillatory behavior in  $\mathbf{s}$  that is similar to that of  $\chi$ . However, due to the broader structure in  $\mathbf{k}$  space, the oscillatory envelope [see Fig. 1(c)] is decaying more rapidly. Moreover, as seen in Figs. 2(d) to 2(f) the gap function is negative at  $\mathbf{s} = 0$ . Here, we are on the top of a very sharp negative peak about  $\mathbf{s} \approx 0$ . This sharp negative peak reflects the strength of the Coulomb repulsion at short length scales.

Beyond the order parameter and the KS pairing potential a third very useful object is the SC condensation energy  $E_{\text{sc}}$ , defined as the difference between the SC and normal state total energy. Equation (1) consists of a kinetic part  $E_{\text{sc}}^{\text{kin}} = \sum_{n\mathbf{k}} \xi_{n\mathbf{k}} (\rho_{n\mathbf{k}}^{\text{sc}} - \rho_{n\mathbf{k}})$ , coming from the change in the occupation numbers of single particle levels from normal ( $\rho_{n\mathbf{k}}$ ) to superconducting ( $\rho_{n\mathbf{k}}^{\text{sc}}$ ), plus the pairing potential contribution given by  $E_{\text{SC}}^{\text{stat}} = - \int d\mathbf{r} \int d\mathbf{r}' \mathcal{E}(\mathbf{r}, \mathbf{r}')$  with the nonlocal static condensation energy density  $\mathcal{E}(\mathbf{r}, \mathbf{r}') = \chi(\mathbf{r}, \mathbf{r}') \Delta_{\mathbf{s}}^*(\mathbf{r}, \mathbf{r}') + \text{c.c.}$  In Fig. 3, [panels (c) and (d)] we show  $\mathcal{E}(\mathbf{R}_0, \mathbf{s})$  for  $\mathbf{R}_0$  in the  $\text{MgB}_2$  B–B– $\sigma$  bond and in the graphane C– $\sigma$  bond. The sharp repulsive Coulomb peak at  $\mathbf{s} \approx \mathbf{0}$  is compensated by the phononic attraction that dominates at larger separations. A sensible, yet nonunique, definition of a *local* condensation energy density [46] is

$$\rho_E(\mathbf{r}) = \int d\mathbf{r}' \mathcal{E}(\mathbf{r}, \mathbf{r}') - \sum_{n\mathbf{k}} \xi_{n\mathbf{k}} [n_{n\mathbf{k}}^{\text{sc}}(\mathbf{r}) - n_{n\mathbf{k}}(\mathbf{r})]. \quad (5)$$

with  $n_{n\mathbf{k}}(\mathbf{r}) = \rho_{n\mathbf{k}} |\varphi_{n\mathbf{k}}(\mathbf{r})|^2$  being the probability density of KS electrons in state  $(n, \mathbf{k})$  [and similarly for  $n_{n\mathbf{k}}^{\text{sc}}(\mathbf{r})$ ]. An important feature of our choice is that it turns out to be positive for all materials studied, this allows us to directly interpret its magnitude as the amount of energy gained in the SC condensation at a point  $\mathbf{r}$ .

Results according to this definition are reported in Fig. 4.  $\rho_E(\mathbf{r})$  includes the competition between the kinetic energy rise due to occupation number change and the energy gain due to the SC pairing. Still its structure resembles closely that of the diagonal of the OP  $\chi(\mathbf{R}, \mathbf{0})$ , apart for the missing negative tails.

In this Letter, in the framework of the density functional theory for superconductors, we performed a real-space

analysis of the superconducting order parameter and the pairing potential (typically only evaluated in reciprocal space), highlighting their relation with the chemical bonding in three anisotropic materials. We showed how the OP structure reflects the underlying pairing mechanism: regions in the unit cell that provide an attractive coupling can be clearly distinguished from those that contribute via a Coulomb renormalization and those that are not coupled. We also show how the chemical bonding structure is utilized to maximize the condensation energy. The broader understanding reached via our real-space analysis may help to better characterize or even design new superconductors, especially in the case of nanostructured systems.

- 
- [1] L. N. Cooper, *Phys. Rev.* **104**, 1189 (1956).
- [2] J. Bardeen, L. N. Cooper, and J. R. Schrieffer, *Phys. Rev.* **108**, 1175 (1957).
- [3] F. London, *Phys. Rev.* **74**, 562 (1948).
- [4] C. Bersier, A. Floris, A. Sanna, G. Profeta, A. Continenza, E. K. U. Gross, and S. Massidda, *Phys. Rev. B* **79**, 104503 (2009).
- [5] H. Rosner, A. Kitaigorodsky, and W. E. Pickett, *Phys. Rev. Lett.* **88**, 127001 (2002).
- [6] P. Townsend and J. Sutton, *Phys. Rev.* **128**, 591 (1962).
- [7] G. I. Rochlin, *Phys. Rev.* **153**, 513 (1967).
- [8] B. L. Blackford and R. H. March, *Phys. Rev.* **186**, 397 (1969).
- [9] A. Floris, A. Sanna, S. Massidda, and E. K. U. Gross, *Phys. Rev. B* **75**, 054508 (2007).
- [10] I. S. Aranson and L. Kramer, *Rev. Mod. Phys.* **74**, 99 (2002).
- [11] L. P. Gor'kov, *Zh. Eksp. Teor. Fiz.* **36**, 1918 (1959) [*Sov. Phys. JETP* **9**, 1364 (1959)].
- [12] P. G. DeGennes, *Superconductivity of Metals and Alloys* (Addison-Wesley, New York, 1989).
- [13] D. K. Morr, *Superconductivity: Conventional and Unconventional Superconductors*, edited by K. H. Bennemann and J. B. Ketterson (Springer-Verlag, Berlin, Heidelberg, 2008).
- [14] M. E. Flatté and D. E. Reynolds, *Phys. Rev. B* **61**, 14810 (2000).
- [15] V. A. Schweigert and F. M. Peeters, *Phys. Rev. B* **60**, 3084 (1999).
- [16] D. K. Morr and N. A. Stavropoulos, *Phys. Rev. Lett.* **92**, 107006 (2004).
- [17] J. Berger and J. Rubinstein, *Connectivity and Superconductivity* (Springer-Verlag, Berlin, Heidelberg, 2000).
- [18] L. N. Oliveira, E. K. U. Gross, and W. Kohn, *Phys. Rev. Lett.* **60**, 2430 (1988).
- [19] M. Lüders, M. A. L. Marques, N. N. Lathiotakis, A. Floris, G. Profeta, L. Fast, A. Continenza, S. Massidda, and E. K. U. Gross, *Phys. Rev. B* **72**, 024545 (2005).
- [20] M. A. L. Marques, M. Lüders, N. N. Lathiotakis, G. Profeta, A. Floris, L. Fast, A. Continenza, E. K. U. Gross, and S. Massidda, *Phys. Rev. B* **72**, 024546 (2005).
- [21] A. Floris, G. Profeta, N. N. Lathiotakis, M. Lüders, M. A. L. Marques, C. Franchini, E. K. U. Gross, A. Continenza, and S. Massidda, *Phys. Rev. Lett.* **94**, 037004 (2005).
- [22] G. Profeta, C. Franchini, N. N. Lathiotakis, A. Floris, A. Sanna, M. A. L. Marques, M. Lüders, S. Massidda, E. K. U. Gross, and A. Continenza, *Phys. Rev. Lett.* **96**, 047003 (2006).
- [23] A. Sanna, G. Profeta, A. Floris, A. Marini, E. K. U. Gross, and S. Massidda, *Phys. Rev. B* **75**, 020511(R) (2007).
- [24] P. Cudazzo, G. Profeta, A. Sanna, A. Floris, A. Continenza, S. Massidda, and E. K. U. Gross, *Phys. Rev. Lett.* **100**, 257001 (2008).
- [25] R. Akashi and R. Arita, *Phys. Rev. Lett.* **111**, 057006 (2013).
- [26] G. M. Eliashberg, *Zh. Eksp. Teor. Fiz.* **38**, 966 (1960) [*Sov. Phys. JETP* **11**, 696 (1960)].
- [27] R. Gonnelli *et al.*, *Phys. Rev. Lett.* **100**, 207004 (2008).
- [28] Coulomb interactions are in this context those occurring in the off-diagonal part of the Nambu self-energy, therefore acting as SC pairing [29].
- [29] P. B. Allen and B. Mitrovic, *Solid State Physics*, edited by F. Seitz (Academic Press, Inc., New York, 1982), Vol. 37, p. 1.
- [30] See Supplemental Material at <http://link.aps.org/supplemental/10.1103/PhysRevLett.115.097002> for details of the electronic and phononic structure calculations and a brief review of the Coulomb renormalization in SCDFT, which includes Refs. [31–37].
- [31] P. Giannozzi *et al.*, *J. Phys. Condens. Matter* **21**, 395502 (2009).
- [32] J. P. Perdew and A. Zunger, *Phys. Rev. B* **23**, 5048 (1981).
- [33] M. Methfessel and A. T. Paxton, *Phys. Rev. B* **40**, 3616 (1989).
- [34] J. P. Perdew and Y. Wang, *Phys. Rev. B* **45**, 13244 (1992).
- [35] C. Lee, W. Yang, and R. G. Parr, *Phys. Rev. B* **37**, 785 (1988).
- [36] J. M. An and W. E. Pickett, *Phys. Rev. Lett.* **86**, 4366 (2001).
- [37] S. Massidda *et al.*, *Supercond. Sci. Technol.* **22**, 034006 (2009).
- [38] D. J. Scalapino, J. R. Schrieffer, and J. W. Wilkins, *Phys. Rev.* **148**, 263 (1966).
- [39] P. Morel and P. W. Anderson, *Phys. Rev.* **125**, 1263 (1962).
- [40] R. S. Gonnelli, D. Daghero, G. A. Umbarino, V. A. Stepanov, J. Jun, S. M. Kazakov, and J. Karpinski, *Phys. Rev. Lett.* **89**, 247004 (2002).
- [41] J. Nagamatsu, N. Nakagawa, T. Muranaka, Y. Zenitani, and J. Akimitsu, *Nature (London)* **410**, 63 (2001).
- [42] A. Sanna *et al.* (to be published).
- [43] G. Savini, A. C. Ferrari, and F. Giustino, *Phys. Rev. Lett.* **105**, 037002 (2010).
- [44] T. E. Weller, M. Ellerby, S. S. Saxena, R. P. Smith, and N. T. Skipper, *Nat. Phys.* **1**, 39 (2005).
- [45] We have normalized the OP shown in Fig. 2 to the maximal values of 42, 97, and 110  $\mu$ /U.c. for MgB<sub>2</sub> (a), CaC<sub>6</sub> (b) and C<sub>2</sub>H<sub>2</sub> (c), respectively. Similarly, we have normalized the KS pair potential to the minimum of 11, 35, and 14  $\mu$ Ry/U.c. in MgB<sub>2</sub> (d), C<sub>2</sub>H<sub>2</sub> (e), and CaC<sub>6</sub> (f).
- [46] The problem of uniqueness in the definition of an energy density is discussed in the context of potential functional theory in A. Cangi, D. Lee, P. Elliott, K. Burke, and E. K. U. Gross, *Phys. Rev. Lett.* **106**, 236404 (2011).
- [47] The maximal values are 0.11, 0.24, and 0.38 nRy/U.c. for Figs. 4(a), 4(b), and 4(c), respectively.